Journal of Alloys and Compounds 509 (2011) 2039–2043

Contents lists available at ScienceDirect

Journal of Alloys and Compounds

journal homepage: www.elsevier.com/locate/jallcom

Enhanced thermoelectric performance in Na-doped *p*-type nonstoichiometric $AgSbTe_2$ compound

B.L. Du[a,b], H. Li[a], X.F. Tang[a,*]

[a] State Key Laboratory of Advanced Technology for Materials Synthesis and Processing, Wuhan University of Technology, Luoshi Road 122#, Wuhan 430070, China
[b] School of Physics and Chemistry, Henan Polytechnic University, Jiaozuo 454000, China

ARTICLE INFO

Article history:
Received 18 July 2010
Received in revised form 10 October 2010
Accepted 22 October 2010
Available online 4 November 2010

Keywords:
Thermoelectric material
Silver antimony telluride
Na
Thermoelectric property

ABSTRACT

Polycrystalline Na-doped *p*-type $AgSbTe_{2+y}$ ($y = 0, 0.02$) compounds were prepared from high purity elements by a melt-quench technique followed by spark plasma sintering. The influences of Na doping and excess Te on the thermoelectric transport properties were investigated. Both Na and Te act as acceptor in $AgSbTe_2$ compound. Substituting Ag with Na has great influence on electron band structure and can enhance the Seebeck coefficient effectively. Adding excess Te in Na-doped samples plays a great role in optimizing the electrical and thermal conductivity. Overall, the thermoelectric performance of the Na doped nonstoichiometric $AgSbTe_2$ samples is greatly improved and a *ZT* of 1.50 is achieved at about 570 K for $Ag_{0.99}Na_{0.01}SbTe_{2.02}$ sample, representing a 30% enhancement with respect to an undoped sample at the same temperature.

1. Introduction

Thermoelectrics are a type of potentially transformative energy conversion technology which can directly convert heat into electricity by using a class of materials known as thermoelectric (TE) materials [1]. It can be used for a variety of applications such as low-grade waste heat scavenging and solar energy harvesting [2]. The efficiency of a TE material is characterized by the dimensionless figure of merit, $ZT = \alpha^2\sigma T/\kappa$, where T is the absolute temperature and α, σ, κ, are the Seebeck coefficient, electrical and thermal conductivity, respectively. The best TE material should be a good electrical conductor and a poor thermal conductor [1].

$AgSbTe_2$ compound is considered as a potential TE material for a long time [3–11] due to its low thermal conductivity ($0.6–0.7\ W\ m^{-1}\ K^{-1}$) [12,13] and now is receiving increasing attentions as an important component of many well-known TE materials [14–20] (such as $(AgSbTe_2)_{1-x}(GeTe)_x$ and $(AgSbTe_2)_{1-x}(PbTe)_x$). Its crystal structure has been identified to be the disordered NaCl type, with Ag and Sb randomly occupying the sodium sites [21]. Theoretical calculations [22,23] show that the effect of Ag/Sb disorder on the holes is small because of the very small contribution to the valence-band-top states from Ag and Sb. However, the big difference in the force constants resulting from the different nature of the Te–Ag and the Te–Sb bonds may introduce strong scattering effect of phonons. So the thermal conductivity of $AgSbTe_2$ compound is limited by the phonon–phonon Umklapp processes to the possible minimum value of bulk materials without special preparation [12]. Moreover, the flat valence band maximum and multi-peak valence band structure are expected to result in a large positive Seebeck coefficient [24]. Low thermal conductivity and large Seebeck coefficient make the $AgSbTe_2$ compound a very promising candidate for high efficiency *p*-type TE applications.

Electronic structure calculations [22,24] indicate that the top of the valence band is predominantly *p* states of the chalcogenides (hybridized with the Sb *p* and Ag *d* states). The broadly dispersed band corresponding to *s* states of Ag comes down and goes below the top of the valence band and the system becomes a pseudogap (or very narrow gap) semiconductor. If we replace Ag with monovalent cation Na with higher *s* state energy, then we should get a narrow band-gap semiconductor for good *p*-type thermoelectrics [22].

Since a monovalent metal atom is a major constituent, *p*-type doping in $AgSbTe_2$ compound is only practicable by changing the stoichiometry between the metals and the chalcogen [25]. Furthermore, the heavy atomic masses and the relative weak chemical bonds between Ag, Sb and Te make all atoms weakly bounding to the $AgSbTe_2$ lattice. Especially, the Ag binding is the weakest, which implies that the formation of an Ag vacancy is energetically easy and therefore may be the source of the *p*-type carriers [24]. So, adding access Te in $AgSbTe_2$ lattice can increase the cation vacancy concentration, and so does the hole concentration. In addition, the point defects accompanying the presence of cation vacancy in the lattice of $AgSbTe_2$ can notably enhance the scattering effects on phonon behavior and result in the reduction of the thermal conductivity. In

* Corresponding author. Tel.: +86 27 87662823; fax: +86 27 87860863.
E-mail address: tangxf@whut.edu.cn (X.F. Tang).

0925-8388/$ – see front matter © 2010 Elsevier B.V. All rights reserved.
doi:10.1016/j.jallcom.2010.10.131

Table 1
Actual composition, room temperature Hall coefficient R_H, hole concentration N, Hall mobility μ_H and reduced effective masses m^*/m_0 of $Na_xAg_{1-x}SbTe_{2+y}$ (x = 0–0.02, y = 0, 0.02) samples.

Nominal composition	Nominal composition	R_H ($\times10^{-8}$ m^3 C^{-1})	N ($\times10^{20}$ cm^{-3})	μ_H (cm^2 V^{-1} s^{-1})	m^*/m_0
$AgSbTe_2$	$Ag_{0.970}Sb_{1.015}Te_2$	40	0.16	75	0.37
$Na_{0.01}Ag_{0.99}SbTe_2$	$Na_{0.009}Ag_{0.975}Sb_{1.030}Te_2$	15	0.61	21	0.52
$Na_{0.02}Ag_{0.98}SbTe_2$	$Na_{0.017}Ag_{0.960}Sb_{1.031}Te_2$	1.9	3.4	2.4	0.96
$Na_{0.01}Ag_{0.99}SbTe_{2.02}$	$Na_{0.009}Ag_{1.009}Sb_{0.980}Te_{2.02}$	4.7	1.3	10	0.19
$Na_{0.02}Ag_{0.98}SbTe_{2.02}$	$Na_{0.018}Ag_{0.968}Sb_{1.026}Te_{2.02}$	1.3	5.0	3.3	0.44

one word, replacing Ag with Na in combination with an appropriate amount of excess Te can make the system a narrow band gap semiconductor with relatively high electrical conductivity.

In present work, Na doped $Na_xAg_{1-x}SbTe_2$ (x = 0–0.05, designated as Na-AST) and $Na_xAg_{1-x}SbTe_{2.02}$ (x = 0–0.02, designated as Na-Te-AST) samples were prepared by melt-quench combining with spark-plasma sintering (SPS) technique. The influence of Na doping and excess Te on phase structure and TE transport properties were studied.

2. Experimental

Starting materials were high purity Na (99.5%), Ag (99.995%), Sb (99.9999%), and Te (99.999%) that were weighed in glove box and loaded into a carbon-coated silica tube. The tube was sealed under vacuum, kept at 973 K for 10 h, and then quenched in brine. The obtained ingots were grounded into powder and SPSed for 5 min under vacuum. The sintering temperature and pressure were 723 K and 35 MPa respectively. Relative densities of all samples were greater than 97%.

The phases of the samples were determined by X-ray diffraction (XRD X'Pert PRO-PANalytical, Cu Kα). The microstructure was investigated by field emission scanning electron microscopy (FESEM, Hitachi, S-4800) with energy dispersive X-ray spectroscopy (EDX). The Hall coefficient R_H was measured by an Accent HL5500PC Hall measurement system. Adopting single-carrier model, the carrier concentration N and Hall mobility μ_H at room temperature were calculated from the formulas ($N = 1/eR_H$, $\mu_H = R_H/\rho$, where e is the electron charge, ρ is the resistivity). High temperature electrical conductivity σ and Seebeck coefficient α were measured simultaneously by the standard four-probe method (Sinkuriko: ZEM-1). Thermal conductivity κ was calculated using the equation $\kappa = \lambda C_p d$ from the thermal diffusivity λ obtained by a flash diffusivity method (LFA 457, Netzsch), specific heat C_p determined by a differential scanning calorimetry method (Q20, TA) and density d obtained by Archimedes method. All measurements were performed in the temperature range from 300 to 700 K.

3. Results and discussion

3.1. Phase composition and microstructure

The actual compositions of sintered samples were examined using EDX on polished surfaces. The differences fall within the expected range compared to nominal formulas (see Table 1), thus all samples are referred as their nominal compositions. Fig. 1 shows XRD patterns of the $Na_xAg_{1-x}SbTe_{2+y}$ samples. All patterns are assigned to a cubic phase (fcc lattice, $Fm\bar{3}m$ group, formula $AgSbTe_2$) except that a diffraction peak splitting is detected in $Na_{0.05}Ag_{0.95}SbTe_2$ specimen (Fig. 1, inset). It indicates that there are two different phases with the same crystal structure and different lattice parameters in $Na_{0.05}Ag_{0.95}SbTe_2$ specimen. Fig. 2 gives the lattice parameter of Na-AST samples. Due to the large covalent radius of Na (0.154 nm) in comparison to Ag (0.134 nm), the lattice parameter increases with the increasing Na substitution fraction. For $Na_{0.05}Ag_{0.95}SbTe_2$ specimen, the deviation from linear dependence of the lattice parameter on x indicates that x = 0.05 has exceeded the solid solubility.

To further investigate the microstructure of the samples, the back-scattered electron image (BESI) analysis and EDX are carried out. Fig. 3 displays the BESI for the polished $Na_{0.02}Ag_{0.98}SbTe_2$ (a) and $Na_{0.05}Ag_{0.95}SbTe_2$ (b) samples. Fig. 4 shows the X-ray maps of Na, Ag, Sb and Te for the polished $Na_{0.02}Ag_{0.98}SbTe_2$ sample. For $Na_{0.02}Ag_{0.98}SbTe_2$ specimen, no relatively dark and bright regions are observed in BESI and elemental maps are uniform. This indicates that there is no obvious segregation of any elements and that all elements are distributed homogeneously in this specimen. However, the BESI shows that the $Na_{0.05}Ag_{0.95}SbTe_2$ specimen is not uniform. Due to the similar atomic number of Ag, Sb and Te, the EDSI is not sensitive to their distribution. So there are Na-rich and Na-poor phases in this sample which correspond to the relatively dark and bright regions. From the results of both XRD and BESI, a conclusion can be drawn: samples with $x \leq 0.02$ form homogeneous solid solutions. In order to exclude the impact of complex phase structure on transport properties, we only present the properties of samples with homogeneous composition in the follow-up discussions.

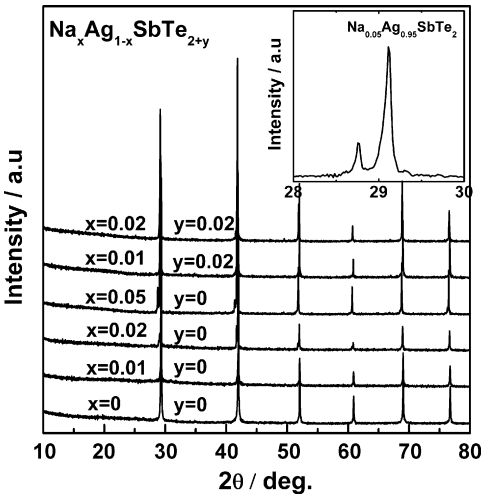

Fig. 1. XRD patterns of $Na_xAg_{1-x}SbTe_{2+y}$ (x = 0–0.05, y = 0, 0.02) samples after SPS. The inset shows the diffraction peak (2 0 0) of $Na_{0.05}Ag_{0.95}SbTe_2$ sample.

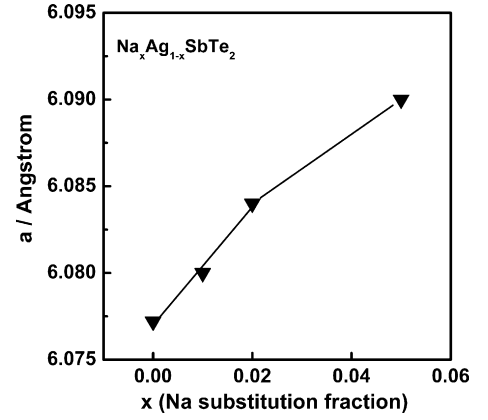

Fig. 2. Lattice parameter as a function of Na substitution fraction for $Na_xAg_{1-x}SbTe_2$ (x = 0–0.05) samples.

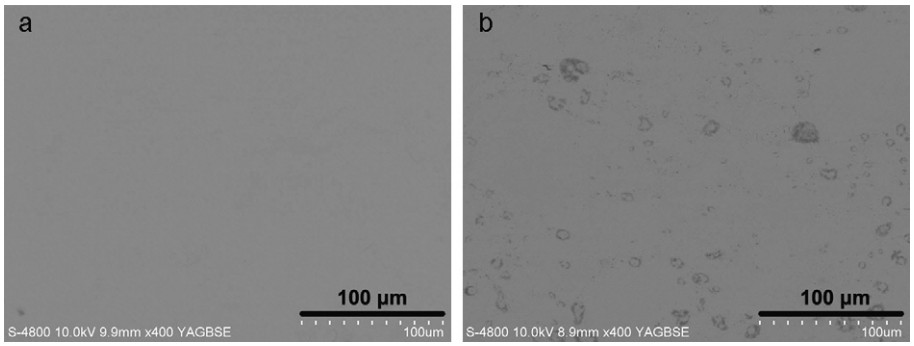

Fig. 3. Back-scattered electron images for (a) $Na_{0.02}Ag_{0.98}SbTe_2$ and (b) $Na_{0.05}Ag_{0.95}SbTe_2$ samples.

3.2. Electrical transport properties

The temperature dependence of the electrical conductivity σ (a) and the Seebeck coefficient α (b) for $Na_xAg_{1-x}SbTe_{2+y}$ compounds are shown in Fig. 5. The Na-AST samples possess lower σ compared with the undoped $AgSbTe_2$ compound at room temperature. Above 600 K, the value of σ is nearly the same as that of the undoped sample due to the intrinsic excitation. However, the Na-Te-AST samples exhibit much higher σ than the Na-AST samples. For $Na_{0.02}Ag_{0.98}SbTe_{2.02}$ specimen, a σ of 2.5×10^4 Sm^{-1} is obtained at about 620 K, representing a 60% enhancement with respect to $AgSbTe_2$ compound at the same temperature.

To explain the electrical transport behavior in this system, the Hall coefficient R_H, carrier concentration N and carrier Hall mobility μ_H of $Na_xAg_{1-x}SbTe_{2+y}$ samples are measured and summarized in Table 1. Compared with the undoped sample, the Na-AST samples display lower Hall coefficient, higher hole concentration and much lower Hall mobility. So Na acts as acceptor in $AgSbTe_2$ compound and generate an acceptor level above the top of valence band. As the increase in carrier concentration is lower than the decrease in Hall mobility, the Na-AST samples display lower σ than the undoped sample. In addition, adding excess Te in Na-AST samples makes the hole concentration increase again. Ye et al. [24] suggest that the formation of Ag^+ vacancy may be a possible origin of the p-type carriers in $AgSbTe_2$ compound. So, when excess Te is added into the Na-AST samples, the Ag+ vacancy concentration increases, and so does the hole concentration.

As shown in Fig. 5b, Seebeck coefficients α of all specimens are positive reflecting the p-type form of transport. At high temperature, the Seebeck coefficients span from 240 to 260 $\mu V\,K^{-1}$, much higher than those of the widely used PbTe and Bi–Te compounds [1]. For Na-AST samples, the values of α at room temperature are much higher than that of the undoped sample. But Na-Te-AST samples exhibit lower α within the whole test temperature range.

Fig. 6 shows the hole concentration N dependence of the Seebeck coefficient α for $Na_xAg_{1-x}SbTe_{2+y}$ samples at room temperature. The Na-AST samples exhibit larger Seebeck coefficient, though they possess much higher hole concentration than the undoped $AgSbTe_2$ sample. Within the framework of a simple parabolic-band model, the Seebeck coefficient and hole concentration are given by the following equations [26]:

$$\alpha = \frac{k_B}{e}\left[\xi_F - \frac{[r+(5/2)]F_{r+3/2}(\xi_F)}{[r+(3/2)]F_{r+1/2}(\xi_F)}\right] \quad (1)$$

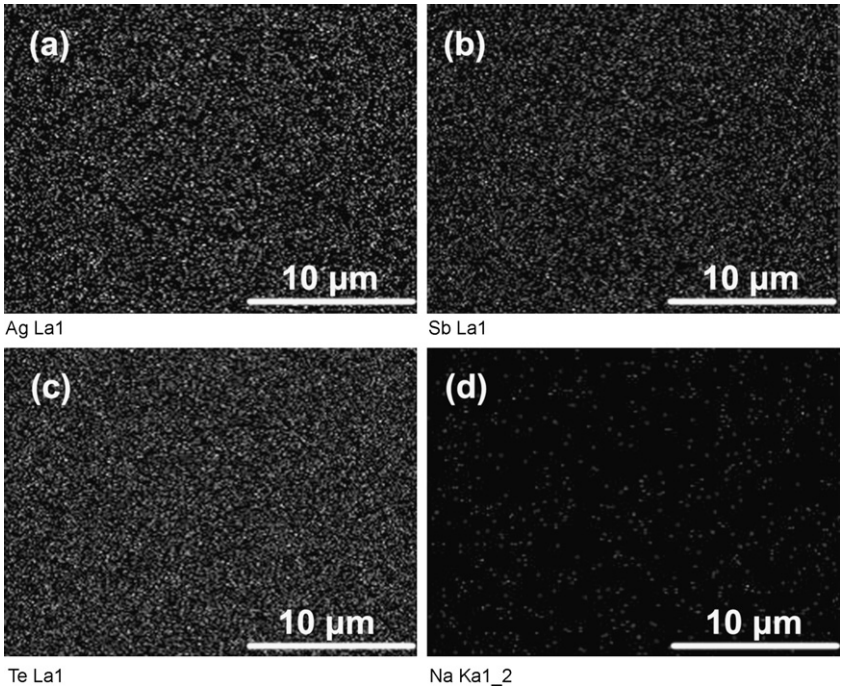

Fig. 4. Elemental distribution for $Na_{0.02}Ag_{0.98}SbTe_2$ sample.

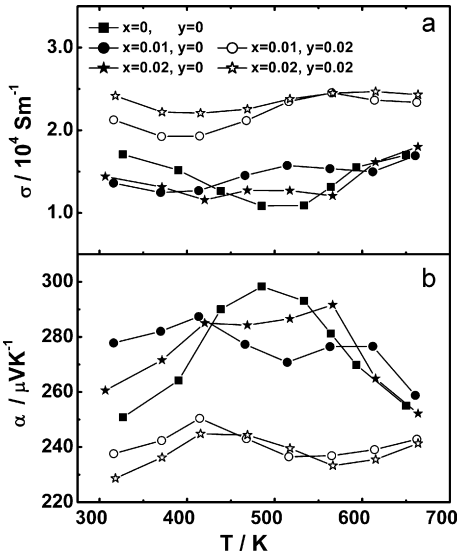

Fig. 5. Temperature dependence of (a) the electrical conductivity and (b) the Seebeck coefficient of $Na_xAg_{1-x}SbTe_{2+y}$ ($x = 0$–0.02, $y = 0$, 0.02) samples.

$$n = \frac{4\pi(2m_0kTm*)^{3/2}}{h^3}F_{1/2}(\xi_F) \quad (2)$$

$$F_i(\xi_F) = \int_0^\infty \frac{x^i dx}{1 + e^{(x-\xi_F)}} \quad (3)$$

where $F_i(x)$ is the Fermi–Dirac integral expressed as Eq. (3), h is the Planck constant, k_B is the Boltzmann constant, ξ_F is the reduced Fermi level $\xi_F = E_F/k_BT$ and r is the scattering factor, which is $-1/2$ for the acoustic phonon scattering in $AgSbTe_2$ compound [3]. Based on the measured Seebeck coefficient and hole concentration, the hole effective masses m^* at room temperature are calculated. As shown in Table 1, Na-AST samples possess larger hole effective mass than undoped sample and the value of m^*/m_0 increase rapidly with the increasing Na substitution fraction. It illustrates that Na doping in $AgSbTe_2$ has great influences on electron band structure and lead to the enhancement in Seebeck coefficient. So replacing Ag with Na is an effective way to increase Seebeck coefficient.

The inset in Fig. 6 shows the power factor PF of $Na_xAg_{1-x}SbTe_{2+y}$ samples at room temperature. Due to the low electrical conductivity, the Na-AST samples exhibit lower PF than the undoped $AgSbTe_2$ sample. However, all the Na-Te-AST samples possess higher PF

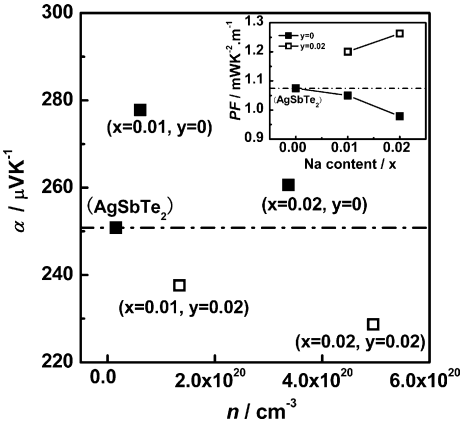

Fig. 6. Hole concentration dependence of Seebeck coefficient for $Na_xAg_{1-x}SbTe_{2+y}$ ($x = 0$–0.02, $y = 0$, 0.02) samples at room temperature. The inset shows the power factor of $Na_xAg_{1-x}SbTe_{2+y}$ samples at room temperature.

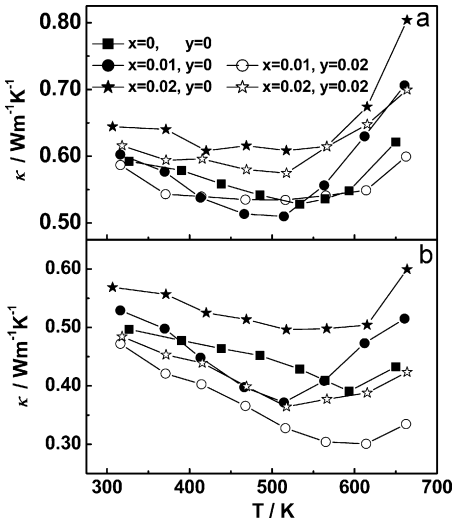

Fig. 7. Temperature dependence of (a) the thermal conductivity and (b) the lattice thermal conductivity of $Na_xAg_{1-x}SbTe_{2+y}$ ($x = 0$–0.02, $y = 0$, 0.02) samples.

than the Na-AST and the undoped samples. For $Ag_{0.98}Na_{0.02}SbTe_{2.02}$ specimen, the value of PF reaches $1.27\,W\,m^{-1}\,K^{-2}$ at room temperature, representing an enhancement of 12% and 30% compared with the $AgSbTe_2$ and $Ag_{0.98}Na_{0.02}SbTe_2$ compounds respectively. In one word, replacing Ag with Na in combination with an appropriate amount of excess Te is an effective way to optimizing the electrical transport properties in $AgSbTe_2$ compound.

3.3. Thermal transport properties

The temperature dependence of the thermal conductivity κ (a) and the lattice thermal conductivity κ_L (b) for $Na_xAg_{1-x}SbTe_{2+y}$ samples are shown in Fig. 7. For all samples, the κ first decreases and then increases with the increasing temperature and the magnitude spans the range from 0.50 to $0.80\,W\,m^{-1}\,K^{-1}$. Near room temperature, bulk of the heat is conducted by long-wavelength acoustic phonons [3] and the rapid increase in thermal conductivity at high temperature may be related to an enhancement in ambipolar thermal conductivity [23].

The lattice thermal conductivity κ_L is estimated using the Wiedemann–Franz law:

$$\kappa_L = \kappa - L\sigma T \quad (4)$$

where $L = 0.7L_0$ and $L_0 = \pi^2/3(k_B/e)^2 = 2.45 \times 10^{-8}\,V^2\,K^{-2}$ [23]. As shown in Fig. 7b, the κ_L of Na-AST samples increases with the increasing Na substitution fraction. Morelli et al. [12] suggest that the low conductivity in $AgSbTe_2$ compound is due to an extreme anharmonicity of the lattice vibrational spectrum resulting from the relatively weak chemical bonds between Ag/Sb–Te and the special bonding arrangement. Because the electronegativity difference between Na and Te (1.17) is much larger than that between Ag and Te (0.17), replacing Ag with Na should result in much stronger bonding between anions and cations. So the anharmonicity of the lattice vibrational spectrum is decreased and a rise in κ_L can be expected. It is interesting that the Na-Te-AST samples possess lower κ_L than undoped sample, especially in high temperature range. For $Ag_{0.99}Na_{0.01}SbTe_{2.02}$ specimen, a κ_{Lmin} of $0.30\,W\,m^{-1}\,K^{-1}$ is reached at 600 K, reaching the theoretical minimum thermal conductivity ($\sim 0.3\,W\,m^{-1}\,K^{-1}$) calculated from the formula presented by Cahill et al. [27]. We ascribe the reduction in the κ_L of Na-Te-AST samples to a strong phonon scattering by cation vacancies accompanying the presence of excess Te in the lattice of $AgSbTe_2$. The lattice defect can introduce strong scattering effect on mid-to-short wavelength

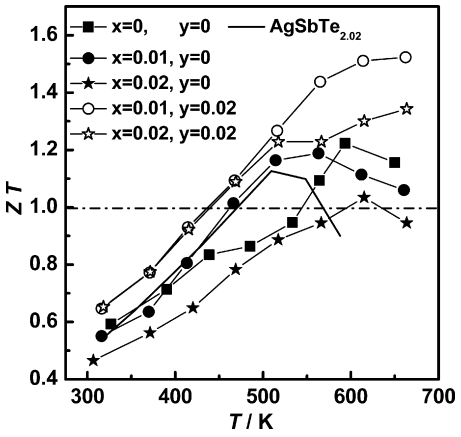

Fig. 8. Temperature dependence of thermoelectric figure of merit *ZT* of $Na_xAg_{1-x}SbTe_{2+y}$ ($x = 0$–0.02, $y = 0$, 0.02) samples.

phonons and can reduce the lattice thermal conductivity at high temperature effectively [28].

3.4. Figure of merit ZT

The dimensionless TE figure of merit *ZT* is calculated based on the measured values of σ, α, and κ using $ZT = \alpha^2\sigma T/\kappa$. Fig. 8 shows the temperature dependence of *ZT* of all $Na_xAg_{1-x}SbTe_{2+y}$ specimens. The *ZT* values of Na-AST samples decrease with the increasing Na substitution fraction. However, Na-Te-AST samples show higher *ZT* values in the whole temperature range. For $Ag_{0.99}Na_{0.01}SbTe_{2.02}$ sample, a *ZT* of 1.50 is observed at 650 K. This value is 30% and 60% higher than those of the undoped $AgSbTe_2$ and Na-AST samples at the same temperature respectively, and is 35% higher than the maximum of *ZT* for $AgSbTe_{2.02}$ specimen.

4. Conclusions

The TE properties of Na-doped $Na_xAg_{1-x}SbTe_2$ and $Na_xAg_{1-x}SbTe_{2.02}$ compounds have been studied. Na acts as acceptor in $AgSbTe_2$ compound. For $x \leq 0.02$, the samples are homogeneous. The TE performance of Na-AST samples is degraded to some extent compared with undoped sample due to the lower electrical conductivity and higher lattice thermal conductivity. However, due to the influence of Na doping on electron band structure, Na-AST samples exhibit higher hole effective mass and Seebeck coefficient than the undoped sample. Adding excess Te in Na-doped samples can increase the hole concentration and electrical conductivity by introducing anion vacancies in specimen, and can lower the lattice thermal conductivity at relatively high temperature range by strong scattering the mid-to-short wavelength phonons. For $Ag_{0.99}Na_{0.01}SbTe_{2.02}$ specimen, a *ZT* of 1.50 is obtained at 650 K, which is 30% higher than that of the undoped $AgSbTe_2$ sample. So replacing Ag with Na in combination with an appropriate amount of excess Te is an effective way to enhance the TE performance of $AgSbTe_2$ compound.

Acknowledgments

This work is sponsored by the National Basic Research Program of China (Grant No. 2007CB607501), the National Science Foundation of China (Grant Nos. 50820145203, 50731006) and the 111 Project (Grant No.B07040).

References

[1] D.M. Rowe, Handbook of Thermoelectrics Macro to Nano, CRC, Boca Raton, FL, 2006.
[2] J. Yang, F. Stabler, J. Electron. Mater. 38 (2009) 1245.
[3] S.N. Zhang, T.J. Zhu, S.H. Yang, C. Yu, X.B. Zhao, Acta Mater. 58 (2010) 4160.
[4] H. Wang, J.-F. Li, M. Zhou, T. Sui, Appl. Phys. Lett. 93 (2008) 202106.
[5] J. Xu, H. Li, B. Du, X. Tang, Q. Zhang, C. Uher, J. Mater. Chem. 20 (2010) 6138.
[6] S.N. Zhang, T.J. Zhu, S.H. Yang, C. Yu, X.B. Zhao, J. Alloys Compd. 499 (2010) 215.
[7] J.D. Sugar, D.L. Medlin, J. Alloys Compd. 478 (2009) 75.
[8] H.-J. Wu, S.-W. Chen, J. Alloys Compd. (2010), doi:10.1016/j.jallcom.2010.09.200.
[9] D.L. Medlin, J.D. Sugar, Scripta Mater. 62 (2010) 379.
[10] P.A. Sharma, J.D. Sugar, D.L. Medlin, J. Appl. Phys. 107 (2010) 113716.
[11] B. Du, H. Li, J. Xu, X. Tang, C. Uher, Chem. Mater. 22 (2010) 5521.
[12] D.T. Morelli, V. Jovovic, J.P. Heremans, Phys. Rev. Lett. 101 (2008) 035901.
[13] E.F. Hockings, J. Phys. Chem. Solids 10 (1959) 341.
[14] S.H. Yang, T.J. Zhu, T. Sun, J. He, S.N. Zhang, X.B. Zhao, Nanotechnology 19 (2008) 245707.
[15] K.F. Hsu, S. Loo, F. Guo, W. Chen, J.S. Dyck, C. Uher, T. Hogan, E.K. Polychroniadis, M.G. Kanatzidis, Science 303 (2004) 818.
[16] A. Gueguen, P.F.P. Poudeu, C.P. Li, S. Moses, C. Uher, J.Q. He, V. Dravid, K.A. Paraskevopoulos, M.G. Kanatzidis, Chem. Mater. 21 (2009) 1683.
[17] P.F.P. Poudeu, J. D'Angelo, A.D. Downey, J.L. Short, T.P. Hogan, M.G. Kanatzidis, Angew. Chem. Int. Ed. 45 (2006) 3835.
[18] F. Ren, E.D. Case, E.J. Timm, E. Lara-Curzio, R.M. Trejo, Acta Mater. 58 (2010) 31.
[19] T. Su, S. Li, H. Ma, X. Li, L. Deng, Y. Yan, W. Guo, X. Jia, J. Alloys Compd. 497 (2010) 432.
[20] J.R. Salvador, J. Yang, X. Shi, H. Wang, A.A. Wereszczak, J. Solid State Chem. 182 (2009) 2088.
[21] R.W. Armstrong, J.W. J Jr., W.A. Tiller, J. Appl. Phys. 31 (1960) 1954.
[22] K. Hoang, S.D. Mahanti, J.R. Salvador, M.G. Kanatzidis, Phys. Rev. Lett. 99 (2007) 156403.
[23] V. Jovovic, J.P. Heremans, Phys. Rev. B 77 (2008) 245204.
[24] L. Ye, H. Khang, A.J. Freeman, S.D. Mahanti, H. Jian, T.M. Tritt, M.G. Kanatzidis, Phys. Rev. B 77 (2008) 245203.
[25] V. Jovovic, J.P. Heremans, J. Electron. Mater. 38 (2009) 1504.
[26] G. Nolas, J. Sharp, H. Goldsmid, Thermoelectrics: Basic Principles and New Materials Developments, Springer, Verlag, 2001.
[27] D.G. Cahill, S.K. Watson, R.O. Pohl, Phys. Rev. B 46 (1992) 6131–6140.
[28] G.J. Snyder, E.S. Toberer, Nat. Mater. 7 (2008) 105.